



Dynamics and stability in the maturation of a eukaryotic virus: a paradigm for chemically programmed large-scale macromolecular reorganization

John E. Johnson¹ · Tatiana Domitrovic² · Tsutomu Matsui³ · Roger Castells-Graells⁴ · George Lomonossoff⁵

Received: 19 September 2020 / Accepted: 2 January 2021 / Published online: 8 March 2021
© The Author(s), under exclusive licence to Springer-Verlag GmbH, AT part of Springer Nature 2021

Abstract

Virus maturation is found in all animal viruses and dsDNA bacteriophages that have been studied. It is a programmed process, cued by cellular environmental factors, that transitions a noninfectious, initial assembly product (provirus) to an infectious particle (virion). Nudaurelia capensis omega virus (NωV) is an ssRNA insect virus with T=4 quasi-symmetry. Over the last 20 years, NωV virus-like particles (VLPs) have been an attractive model for the detailed study of maturation. The novel feature of the system is the progressive transition from procapsid to capsid controlled by pH. Homogeneous populations of maturation intermediates can be readily produced at arbitrary intervals by adjusting the pH between 7.6 and 5.0. These intermediates were investigated using biochemical and biophysical methods to create a stop-frame transition series of this complex process. The studies reviewed here characterized the large-scale subunit reorganization during maturation (the particle changes size from 48 nm to 41 nm) as well as the mechanism of a maturation cleavage, a time-resolved study of cleavage site formation, and specific roles of quasi-equivalent subunits in the release of membrane lytic peptides required for cellular entry.

Introduction to virus maturation

Virus maturation is a phenomenon that is associated with all animal viruses and dsDNA bacteriophage that have been studied to date. It involves a programmed process in which an initial, noninfectious assembly product (provirus) transitions to an infectious particle (virion). Rationalizing the need for maturation can be approached from more than one

perspective, and they may be related. There is the advantage of not producing an infectious particle in a cell that is already infected. By activating particle infectivity through cues associated with leaving the cell, or in cells dying due to the infection (apoptosis), the virus maximizes efficient compromise of the host by infecting only previously uninfected cells. A second may involve assembly and stability. Many intracellular molecular interactions are weak, facilitating annealing to activate specific processes associated with the

Handling Editor: Marc H. V. Van Regenmortel.

John E. Johnson
jackj@scripps.edu

Tatiana Domitrovic
domitrovic@micro.ufrj.br

Tsutomu Matsui
tmatsui@slac.stanford.edu

Roger Castells-Graells
rcastellsg@ucla.edu

George Lomonossoff
george.lomonossoff@jic.ac.u

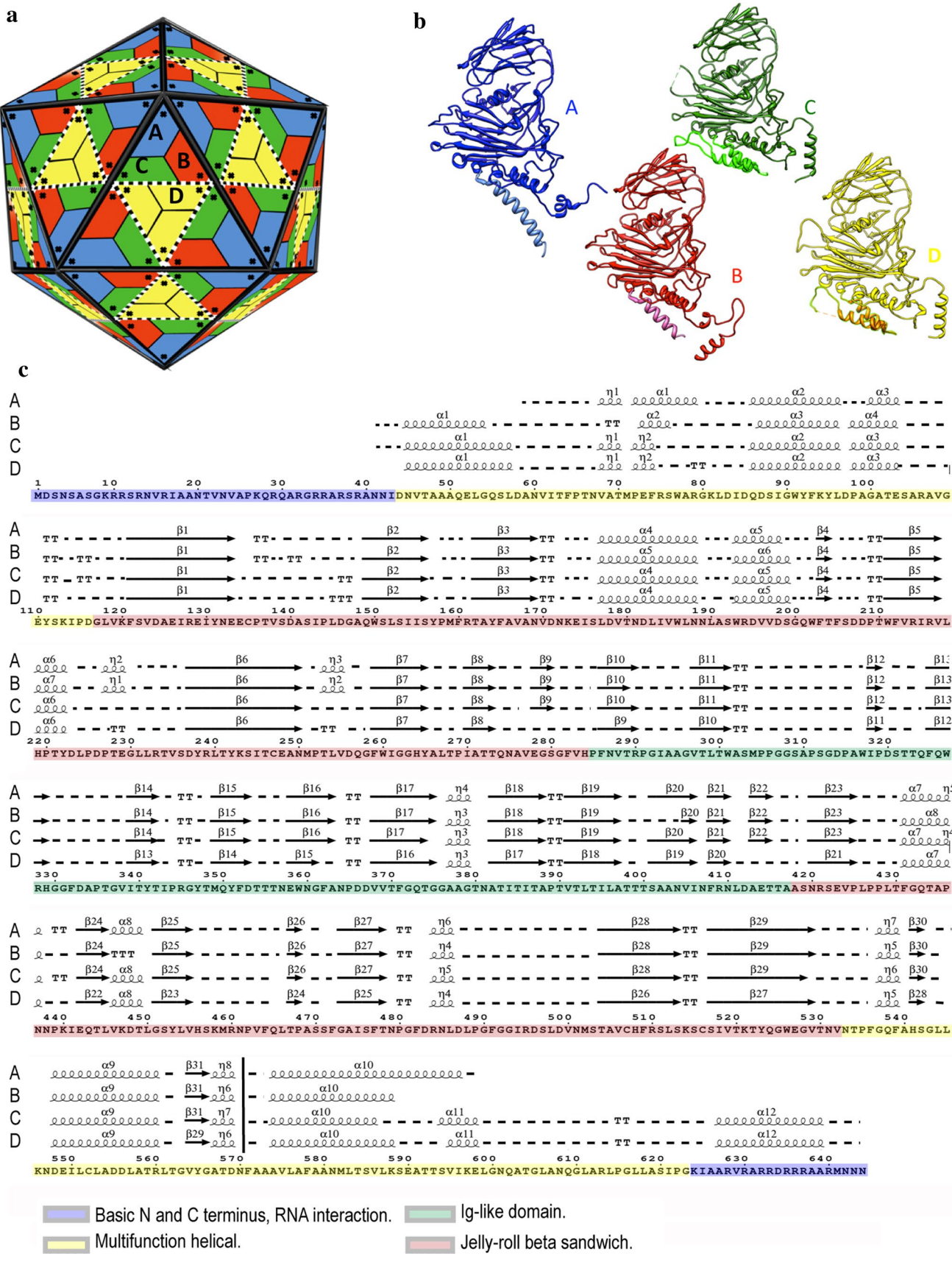
² Universidade Federal do Rio de Janeiro, Instituto de Microbiologia Paulo de Góes, Rio de Janeiro 21941-902, Brazil

³ Stanford Synchrotron Radiation Lightsource (SSRL), 2575 Sand Hill Rd, MS69, Menlo Park, CA 94025, USA

⁴ Department of Chemistry and Biochemistry, University of California, Los Angeles, 611 Charles Young Dr. East, Los Angeles, CA 90095-1569, USA

⁵ John Innes Centre, The John Innes Centre, Norwich Research Park, Norwich NR4 7UH, UK

¹ Department of Integrative Structural and Computational Biology, The Scripps Research Institute, 10550 N. Torrey Pines Rd., La Jolla, CA 92037, USA



◀Fig. 1 a. N ω V has a bipartite RNA genome with both segments packaged in a single particle and each expressing a single protein. RNA1 expresses the RNA-directed RNA polymerase (RDRP), and RNA2 expresses protein α , the precursor of β and γ in the mature virus particle. The mature virion is 410 Å in diameter and is composed of 240 subunits with identical sequences and arranged with T=4 quasi-symmetry. b. The 2.8 Å crystal structure showed that the four subunits in the icosahedral asymmetric unit (labeled by color and letter) are closely similar in tertiary structure and formed by a viral jelly roll with an IgG domain inserted between two strands of the jelly roll. c. The sequence of protein α and a comparison of structures in the four subunits. α is cleaved between residues 570 and 571 to produce β (1-570) and γ (571-644). The color coding indicates the different secondary structure domains as indicated. The portions in yellow have different structures in one or more of the subunits, indicating that the same sequences have different structure. "V" represents helices, "=" represents strands, and "..." represents coils and turns.

interaction [1]. It can be argued that assembly of hundreds of subunits into a particle is fraught with “traps” if the interactions are too strong, whereas it is facilitated by weak interactions that are self-correcting [2]. While weak interactions are all that are required for the formation of intracellular molecular complexes, virus particles have an extracellular component of their life cycle where the environment is harsh, requiring robust particle stability. An effective solution is to construct a relatively unstable initial particle, ideal for correct assembly, that incorporates an externally cued chemical program that makes it more stable. As discussed later, it will be clear that conferring infectivity and greater stability are often related when the process is fully understood.

Maturation has been extensively investigated in dsDNA bacteriophages [3] as well as medically important viruses such as human immunodeficiency virus (HIV) [4] and flaviviruses [5]. Highly successful antiviral agents for HIV are protease inhibitors [6] that prevent viral polyprotein (Gag) cleavages required for maturation that leads to ribonucleoprotein morphological changes and infectivity. Maturation frequently involves large-scale particle reorganization, as shown in some detail with dengue virus, where moderate-to-high-resolution electron cryo-microscopy (cryoEM) structures of the provirion and virion were determined as a result of particle icosahedral symmetry [7].

The biophysical study of intermediates in virus maturation is required to understand the code of the maturation program. This has proven difficult for most well-studied systems. Maturation of dsDNA bacteriophage tends to be binary with one or more two-state events in the route to maturation. Intermediates between states are fleetingly populated and can only be studied by single-particle methods, prohibiting their high-resolution analysis. These transitions are analogous to popcorn, where the kernel matures to the popped state in a fraction of a second (<https://www.youtube.com/watch?v=FSZd33awqQk>) with no populated intermediates. A second problem is the lack of homogeneity of the particle population. This was encountered with dengue

virus [7]. Although the maturation of the ensemble appears to be smooth, examination of individual particles reveals that they are partially matured and at different stages. These are known as “mosaic particles” and are, again, difficult to image at high resolution.

High-resolution investigation of maturation requires the capacity to populate any intermediate on the pathway in a stable and homogeneous mode so that it can be frozen (both literally and figuratively) and visualized by high-resolution cryo-EM. The goal is to generate a movie of the maturation process (at arbitrary resolution of the intermediates) that allows the code of the maturation program to be read, line by line, with associated understanding of the basic physics and chemistry of the biological phenomena. Achieving such a goal requires a novel system with the properties described above, and, to date, one has not been found among the medically important viruses that are heavily investigated.

Nudaurelia capensis ω virus (N ω V): a model system for icosahedral virus maturation

Investigations of members of the family *Alphatetraviridae* using X-ray crystallography and cryoEM have been underway since 1985. Crystalline tetraviruses were initially characterized in 1990 employing authentic virus purified from pine emperor larvae in South Africa [8, 9]. The N ω V capsid protein gene sequence [10] and near-atomic-resolution structure of authentic, mature N ω V were published in the next five years [11]. Later, the structure was refined [12], and its implications were fully interpreted. N ω V is a 41-nm virus that infects *Lepidoptera* and has an icosahedral capsid with a T=4 quasi-equivalent surface lattice (240 chemically identical subunits/particle) and packages a bipartite ssRNA genome. RNA1 encodes the RNA-directed RNA polymerase (RdRp), and RNA2 encodes the precursor to the mature capsid protein. The N ω V-encoded subunit is comprised of 644 amino acids. The crystal structure showed an ~5 Å break in the polypeptide chain between residues 570 and 571 in all subunits, explaining the doublet observed in SDS gels of the virus, where bands at a mass of ~70 kDa (faint) and ~62 kDa (strong) were observed [13]. Combining information from the structure and sequence, the following description emerged: as dictated by the surface lattice, there are four independent (not related by strict symmetry) subunits in the icosahedral asymmetric unit designated as A, forming pentamers (with four adjacent subunits related by 5-fold icosahedral symmetry to A), and B, C, and D, forming hexamers (with equivalent residues related by 2-fold icosahedral symmetry). Residues 1-44 contain 11 basic residues, and the region is invisible in all of the subunits; residues 624-644 contain nine basic residues that are visible only in the C and D subunits; residues 45-118 and 533-623 form structures

that have differences between subunits; residues 118–284 and 421–531 form a viral jelly roll with an Ig domain (288–419) inserted between two strands, and these structures are precisely superimposable in all four subunits. Figure 1 illustrates these observations.

Production of N_oV virus-like particles (VLPs)

A ten-year effort to determine the structure of N_oV appeared destined to have only a modest impact on virology, as it proved impossible to find a cell line in which to propagate and investigate the N_oV life cycle; N_oV would grow only in the host organism (pine emperor moth larvae). Discouraged, other approaches were considered to learn more about the assembly of the virus that could be related to the structure. Employing an approach used successfully for the T=3 ssRNA-containing Flock House virus (FHV) [14], *Spodoptera frugiperda* line 1 cells infected with recombinant baculoviruses containing the gene for wild-type N_oV capsid protein expressed high yields of virus-like N_oV particles [13]. The initial excitement about the positive detection of particles was soon tempered by the observation that the purified particles did not resemble the 41-nm, icosahedral-shaped virus structure. The expressed particles were spherical with a diameter of 48 nm and showed only the full-length subunit mass of ~70 kDa in SDS gels, indicating an assembly defect that prevented the cleavage. Deeply discouraged, all aspects of the crystallization and expression were reviewed. A striking difference was identified. The virus was purified, stored, and crystallized at pH 5.0 and the VLPs were maintained at

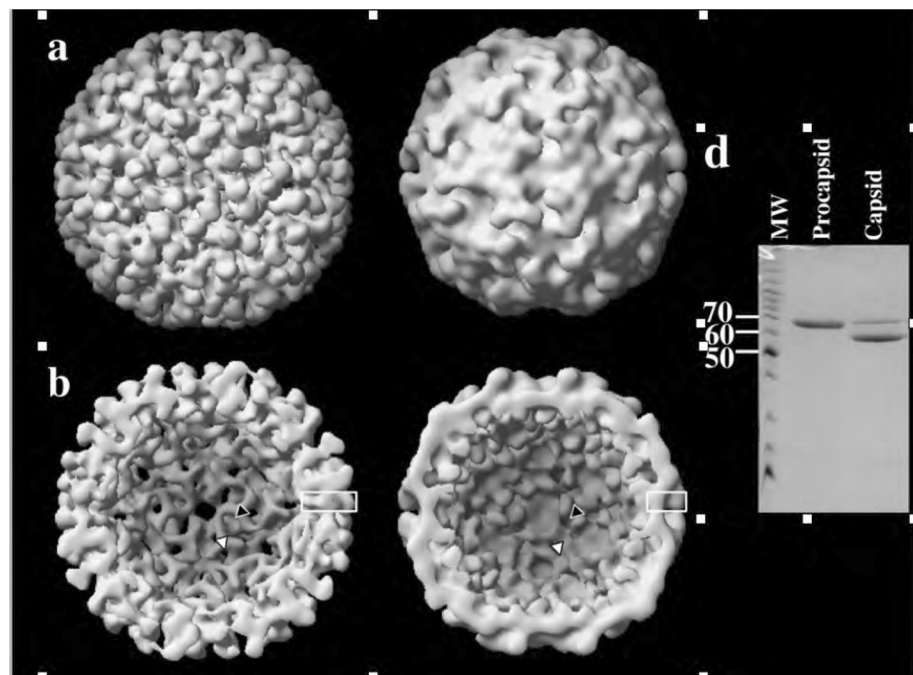
pH 7.6 during expression and purification. To emulate the crystallization conditions, the pH of the VLPs was lowered from 7.6 to 5.0 with a resulting formation of 41-nm, icosahedral-shaped particles and the concomitant appearance of the characteristic doublet of the virus coat protein on an SDS gel [15] (Fig. 2). This demonstrated that the cleavage was autocatalytic within the particle, since the particles were highly purified with no detectable foreign protein. The VLPs at pH 5.0 were indistinguishable from authentic virus particles by negative-stain EM and SDS gel electrophoresis.

This observation immediately suggested a number of questions that were addressed systematically. What is the rate of the conformational change? Was the change continuous or binary (popcorn)? At a given intermediate pH, were all the particles in the ensemble the same or were there different populations of particles (mosaic ensemble)? What is the rate of the cleavage, and could it be characterized using a kinetic model? Did the cleavage affect the final state of the particle? What purpose did the cleavage serve for the particle, for infectivity?

Solution small-angle X-ray scattering (SAXS) of N_oV maturation

SAXS is a very sensitive method to determine the size of spherical particles. There is an accurate expression for the calculated scattering pattern of a sphere that depends on the particle radius (Fig. 3). The particle radius can be computed with high precision when the difference between the observed and calculated spherical SAXS patterns is

Fig. 2 Three-dimensional, surface-shaded (a) full particle and (b) sectioned views of the procapsid (left) and capsid (right) of N_oV VLPs viewed down a 2-fold symmetry axis, with 3-fold (black triangle) and quasi 3-fold (white triangle) axes marked in panel b. The procapsid is 480 Å, rounded, and porous, while the mature capsid is 410 Å, angular, and has a solid shell. (d) SDS-PAGE gel showing that the procapsid sample contains α (70 kDa uncleaved) coat protein, while the capsid contains mostly β (62 kDa) and γ (8 kDa) (not visible) coat protein fragments, which result from autoproteolysis upon lowering of the pH to 5.0.



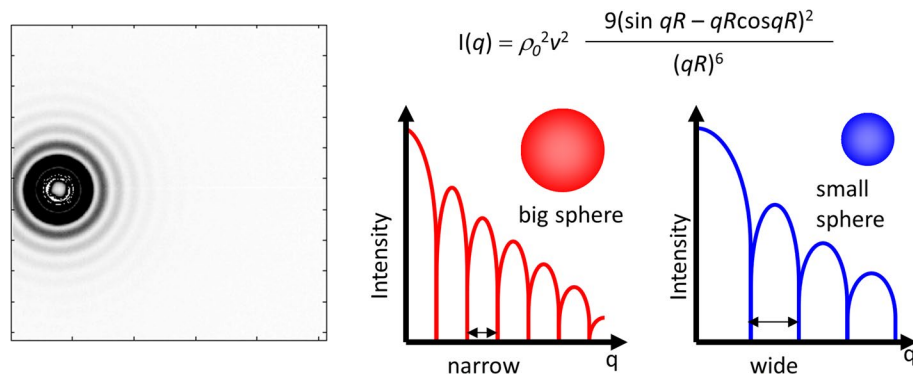


Fig. 3 Small-angle X-ray scattering (SAXS) determination of sphere sizes. Left: a typical SAXS pattern from a solution of spherical particles. The pattern appears as a “bull’s eye” with dark circles of maximum intensity separated by gaps with weak scattering (nodes). Typically, the patterns are circularly symmetrical, so they are averaged at constant radius and plotted as one-dimensional scattering patterns as shown in the plots on the right. The plots show intensity (I , ordinate)

vs. scattering angle (q , abscissa). The formula shows the mathematical model for the intensity distribution of a uniform sphere as a function of its radius. With the R^6 in the denominator, it is clear that the larger the radius, the more compact the pattern, as shown in cartoon fashion in the plots. The formula allows for very precise determination of radii from the scattering pattern.

minimized. Initial experiments were designed with a pH change stop/flow apparatus allowing changes to occur rapidly with a fast SAXS readout. It was determined that, when the pH was changed from 7.6 to 5.0 “instantaneously”, the structural transition was faster than the “dead time” of the instrument, ~100 ms. Clearly changing the electrostatics of the particle with a pH drop leads to an unobstructed rapid transition from one state to the other [16]. This was explored further by carefully adjusting

the pH to intermediate values between 7.6 and 5.0 and allowing the system to equilibrate for 3 days. Figure 4 demonstrates that the transition is continuous and not binary (popcorn) as found in the bacteriophage HK97 [17] (shown for comparison in the figure). SAXS patterns were collected, and spherical modeling was done between 360 Å and 180 Å resolution, where the first two nodes in the pattern occur and where the scattering from the particle is nearly a true, uniform sphere (Fig. 5). The modelling with

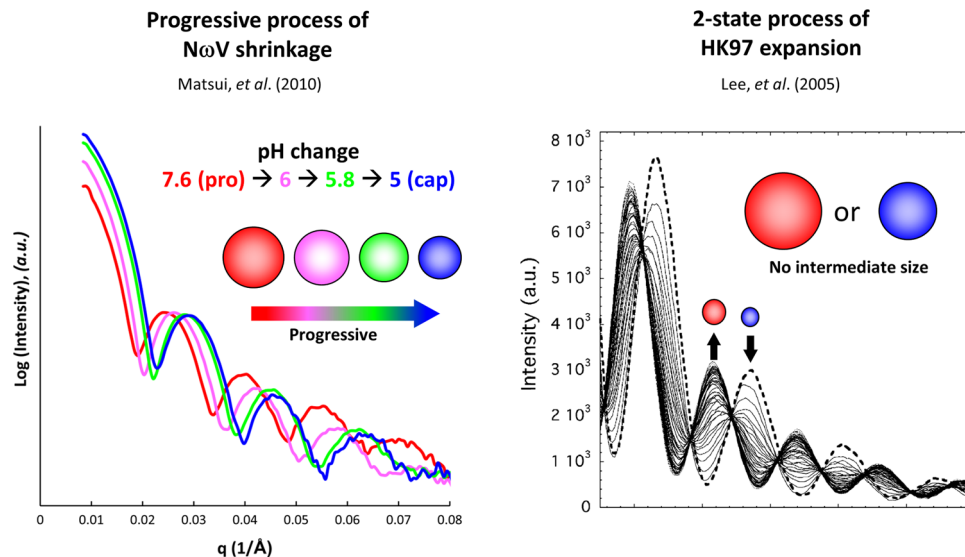
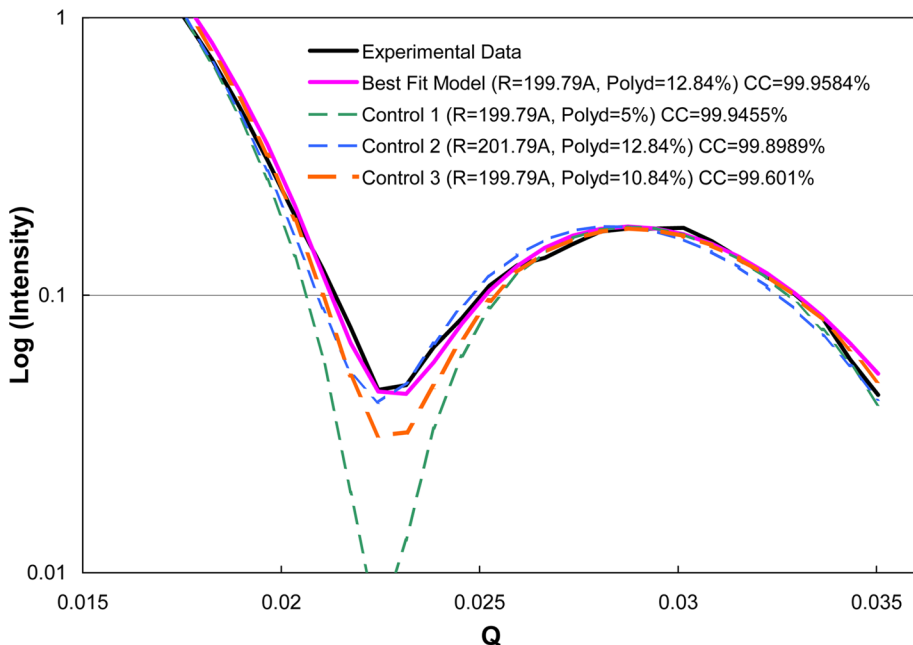


Fig. 4 Comparison of SAXS patterns from progressive and binary transitions observed in virus maturation. On the left are color-coded patterns from NoV virus-like particles at pH 7.6 (procapsids) and 5 (capsids) and at intermediate pH values of 6 and 5.8. The scattering pattern moves smoothly to the left from 5 to 7.6 as the particle radius gets smaller [21]. In contrast, in the time-resolved pattern of

HK97 scattering during the procapsid-to-capsid transition (capsid is larger than the procapsid in this case), there are isosbestic points in the pattern, indicating that the system is two-state with no populated intermediates between the two states [17]. This is an example of a “popcorn” transition described in the text, and the patterns at different time points show the fraction of the two states at any moment.

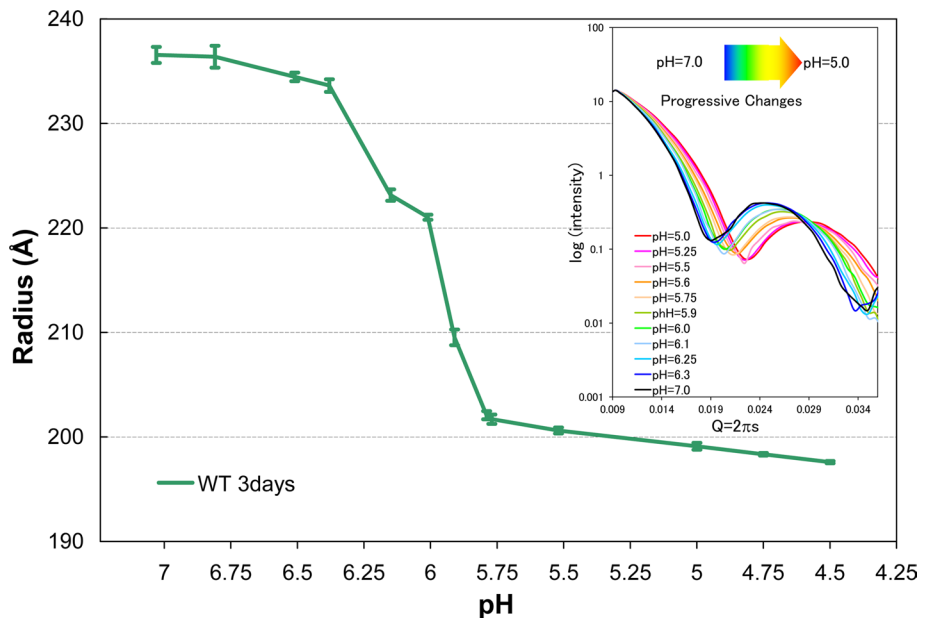
Fig. 5 The fit of the model (Fig. 3 equation) to the data is extremely sensitive in the low-resolution SAXS pattern. The data show that even a 5% change in polydispersity (Control 1) or a small change in radius (Control 2) or both (Control 3) significantly changes the correlation of the model to the observed data. The analysis explains the apparent conundrum that data at 209 Å resolution can discern a difference of 2 Å in radius. The explanation is that the equation in Fig. 3 allows the fit of a precise model to the observed data.



the non-linear fitting program MIXTURE (a component of the SAXS analysis program PRIMUS [18]) allowed quantitative analysis of a uniform sphere size and a polydispersity factor as well as interparticle interference effects [19]. The analysis showed that at pH values between 6.5 and 5.8 the ensemble of particles displayed large differences in size with small changes in pH and that the population at any given pH had a low polydispersity (~12%). These data indicate that the transition is continuous with highly homogeneous intermediate populations. Figure 5

also shows that the parameters for fitting the model to the data are extremely sensitive with even small changes from optimal generating significant discrepancies between the model and the data, explaining the exceptionally small standard deviations (~2 Å on average) for the particle sizes in triplicate experiments. The particle size at different pH values allowed the calculation of a titration curve for the transition, as shown in Figure 6, where the particle size functions as the “indicator” and demonstrates that the overall pK_a for the transition is 6.0.

Fig. 6 A titration curve for N_ωV VLPs employing the particle radius as the “indicator”. Note that the particles in this plot were incubated for 3 days and were at equilibrium when the SAXS data were collected. The SAXS patterns at each pH value are shown in the upper right, demonstrating the smooth progression of the pH-induced transition. The pK_a for the particle is approximately 6. The standard deviations of the radii were determined from three independent SAXS measurements of different samples at each pH value.



Autocatalytic cleavage of N_ωV subunits during maturation

The next aspect of the transition analyzed was the cleavage between residues Asn570 and Phe571. It was straightforward to measure the kinetics of the reaction when the pH was decreased from 7.6 to 5.0 (or other pH values between 4 and 5.5), as cleavage was slow and was easily monitored by SDS gel analysis at time points in the reaction (Fig. 7). The reaction was optimal at pH 5.0, but the kinetics were unexpected. Approximately half the subunits were cleaved in the first 30 minutes, but it took many hours for the remaining subunits to be cleaved [19]. This immediately suggested that the different subunits in the icosahedral asymmetric unit may be cleaved at different rates, although in the crystal structure of the virus the cleavage site and surroundings were superimposable in the four subunits.

In order to better understand the cleavage reaction, it was important to establish a mechanism. Previously, the mechanism of the FHV maturation cleavage was recognized as requiring an Asp that functioned as a base that attached to the side chain proton of the Asn residue at the cleavage site, resulting in the nucleophilic attack of the side chain on the

carbonyl carbon of the main chain with the formation of a cyclic imide and subsequent cleavage after the Asn. The environment of the cleavage site for N_ωV was strikingly similar to that of FHV, with a Glu residue playing the role of the base. In Figure 8, panels a and b show the environment of the cleavage site in N_ωV, and panel 8c shows the mechanism. The outline of the mechanism was confirmed by mutagenesis [20].

Particle annealing and subunit cleavage during maturation at intermediate pH values

The next problem addressed was the association of pH and the rate at which particles become compact at the pH values shown in Figure 6. The particle sizes at 1 minute and 3 days were determined and are compared in Figure 9, demonstrating that there is an annealing process during the change in particle size at pH values between 6.0 and 5.1 [19]. By contrast, there is essentially no difference between 1 minute and 3 days at pH 5.0 and below. This is consistent with stop-flow experiments in which the particle reached the compact state in less than 100 ms at pH 5.0.

Fig. 7 a. The kinetics of the autocatalytic cleavage of N_ωV VLPs when the pH was lowered from 7.6 to the indicated pH as rapidly as possible. b. Cleavage was monitored by the appearance of the 62-kDa β polypeptide and quantitated by scanning the gels. The data were plotted as the fraction of the subunits not cleaved at each time point. While the cleavage showed some pH dependence, its striking feature was that approximately half of the subunits were cleaved in 30 minutes, whereas the remainder required hours for full cleavage.

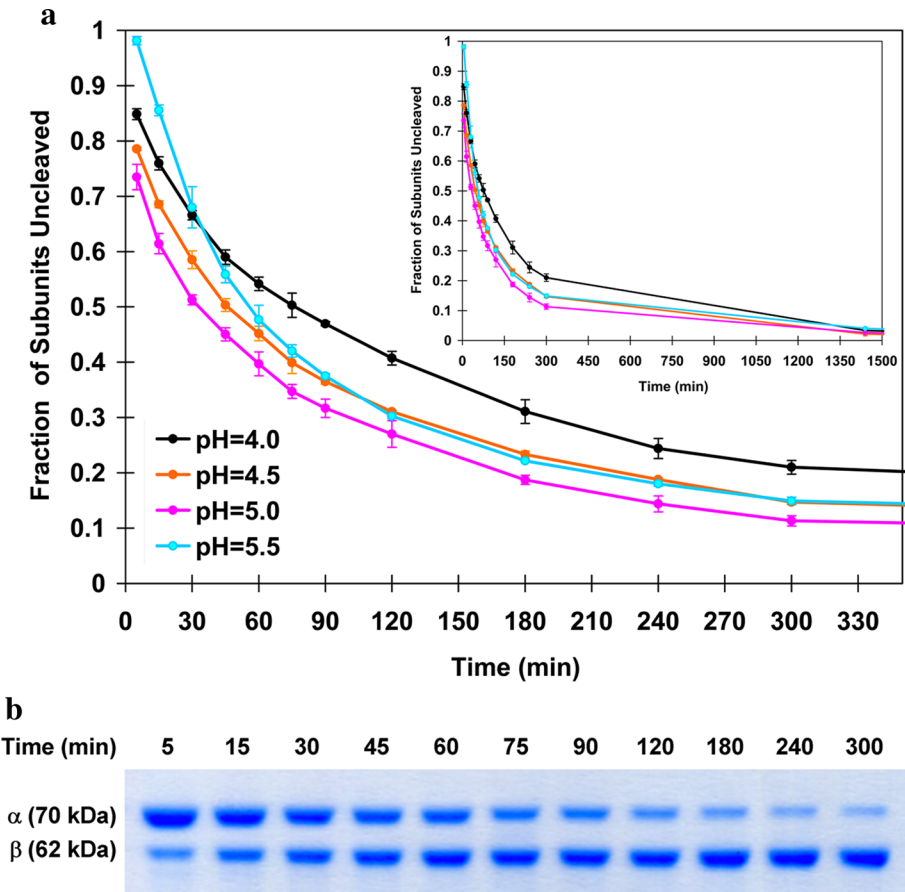
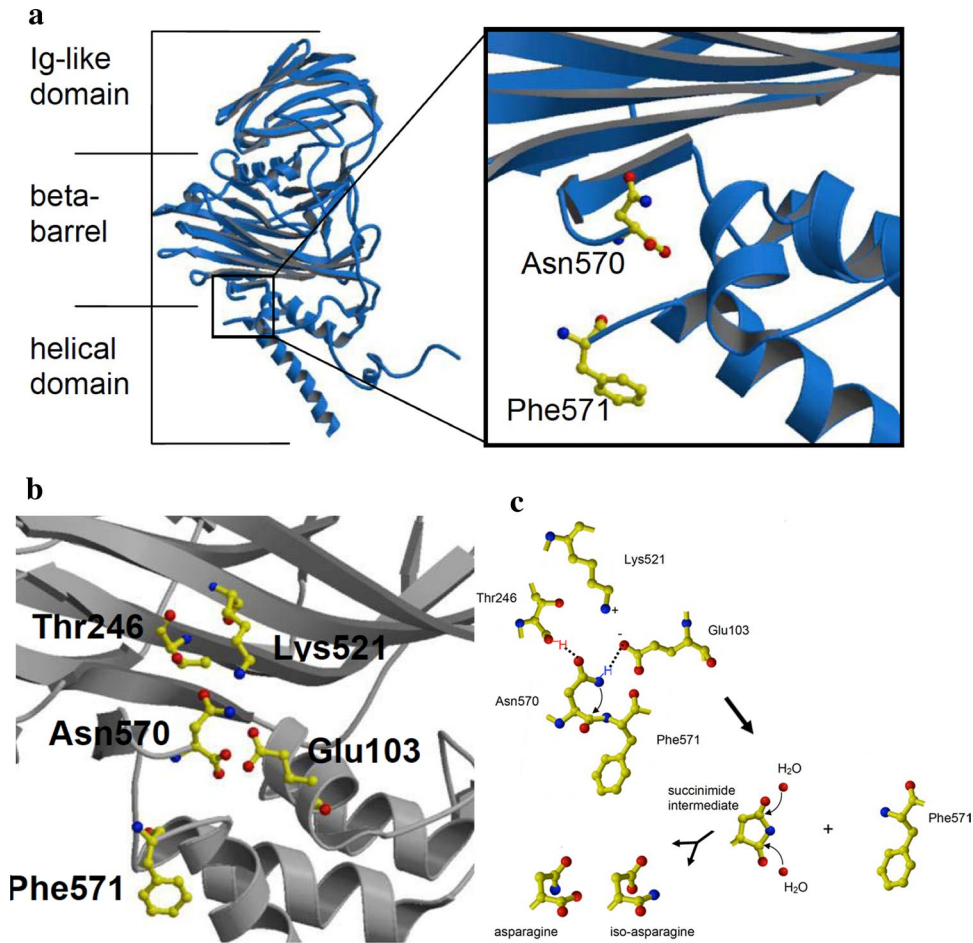


Fig. 8 Top: The cleavage site in subunit A of N ω V. The top represents the outside of the particle, and the bottom is the region where the RNA is located. The cleavage site is not accessible from outside of the particle. An expanded view of the cleavage site is shown at the right. Middle: A detailed view of the cleavage site showing important hydrogen bonds in the region. Glu103 and Asn570 are both required for the cleavage activity. Mutation of other highlighted residues slows the activity but does not stop it [33]. Bottom: The proposed mechanism for the cleavage based on known degradation pathways in the lens proteins of the eye leading to cataracts [34]



Each of the data points in Figure 9 was tested for evidence of cleavage. As suggested by the kinetics in Figure 7, where the first accurately measured time point was at 5 minutes, no cleavage was detected in any of the samples (even at pH 4.5) within 1 minute. The data for the 3-day incubation were more interesting. Cleavage only began at pH 5.8 or below with the particle radius below 220 Å. At pH values above 5.5 the cleavage reaction did not go to completion in 3 days, with roughly 50% of the subunits cleaved at that time point. At pH 5.5 and below, the cleavage was essentially 100% complete within 3 days. The data point at pH 5.5 was examined further with time-resolved SAXS and cleavage kinetics as shown in Figure 10, where the particle size (ordinate) is plotted against the fraction of subunits cleaved (abscissa). There is a clear correlation of particle size with the number of cleavages, indicating that, at this pH, the subunits that are not cleaved prevent the particle from reaching the final compact state, suggesting that they form a type of scaffold that must collapse due to cleavage for the particle to reach the “ground state” [21].

Particle size reversibility and particle stabilization by subunit cleavage

The correlation of particle size and subunit cleavage raised additional questions concerning the role of cleavage and particle dynamics. Further investigation of the procapsid demonstrated reversibility of the particle size change at pH values where no cleavage could occur (above 5.8) when the pH was raised back to 7.6. However, below pH 5.8, there was no reversibility after a 3-day incubation of the particles. The role of cleavage in controlling particle size reversibility was tested by making a non-cleaving mutation (Asn570Thr). This mutation allowed the entire maturation (at pH 5.0) to be mostly reversible (a small population of particles did not return to the fully expanded state in 24 hours of pH 7.6 incubation), demonstrating a critical role of cleavage in stabilizing the compact state [20].

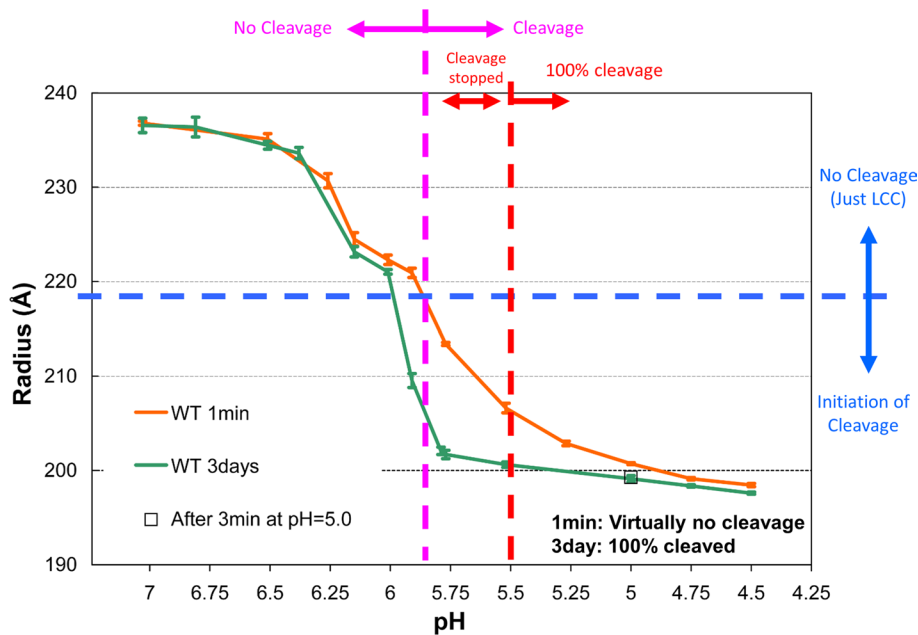
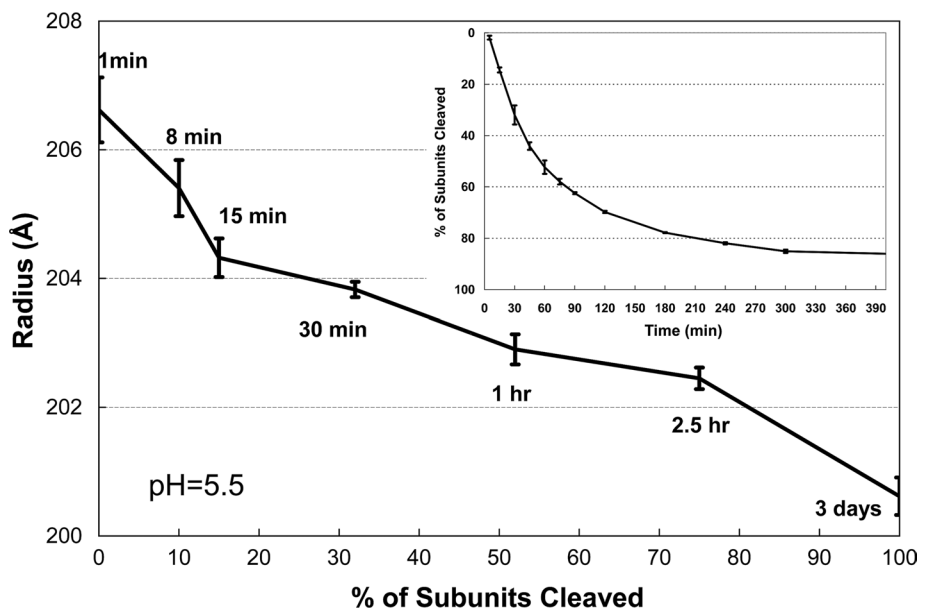


Fig. 9 Time-resolved dynamics of NoV VLP maturation. SAXS data were collected 1 minute after lowering the pH to the specified value and compared with SAXS data after 3 days at the specified pH. At pH values above 5, there is a clear period of annealing as the particles move from an initial state at a given pH to the final state. Between pH values of 5.8 and 5.4, the difference in the initial radius and final radius is large. The figure also relates the particle state and size to cleavage. Above pH 5.8, there is no detectable cleavage in 3 days,

although the particle has clearly undergone significant size reduction. Between pH values of 5.8 and 5.6, cleavage initiates but does not complete in 3 days. Below pH 5.5, cleavage goes to near completion in 3 days. At pH 5, the particle transitions to its final state in just 3 minutes. These data suggest that reduction in charge repulsion at lower pH values allows the particle to rapidly achieve the “ground state”.

Fig. 10 Time-resolved analysis of the particle size change at pH 5.5 and associated cleavage of the subunits (inset). There is a correlation between the fraction of subunits cleaved and the particle size, suggesting that the uncleaved subunits function as a scaffold supporting the particle architecture and, as the subunits are cleaved, the scaffold collapses allowing the particle to decrease in size.



A simplified electrostatic model of particle maturation

A model for the data presented thus far is summarized as a cartoon in Figure 11. The atomic model of the virus

shows that the subunit surfaces are covered with many acidic residues that are negatively charged at neutral pH, providing a large, repulsive electrostatic potential and a rationale for the existence of the large, porous particle at pH 7.6. The subunits are held in proximity by strong

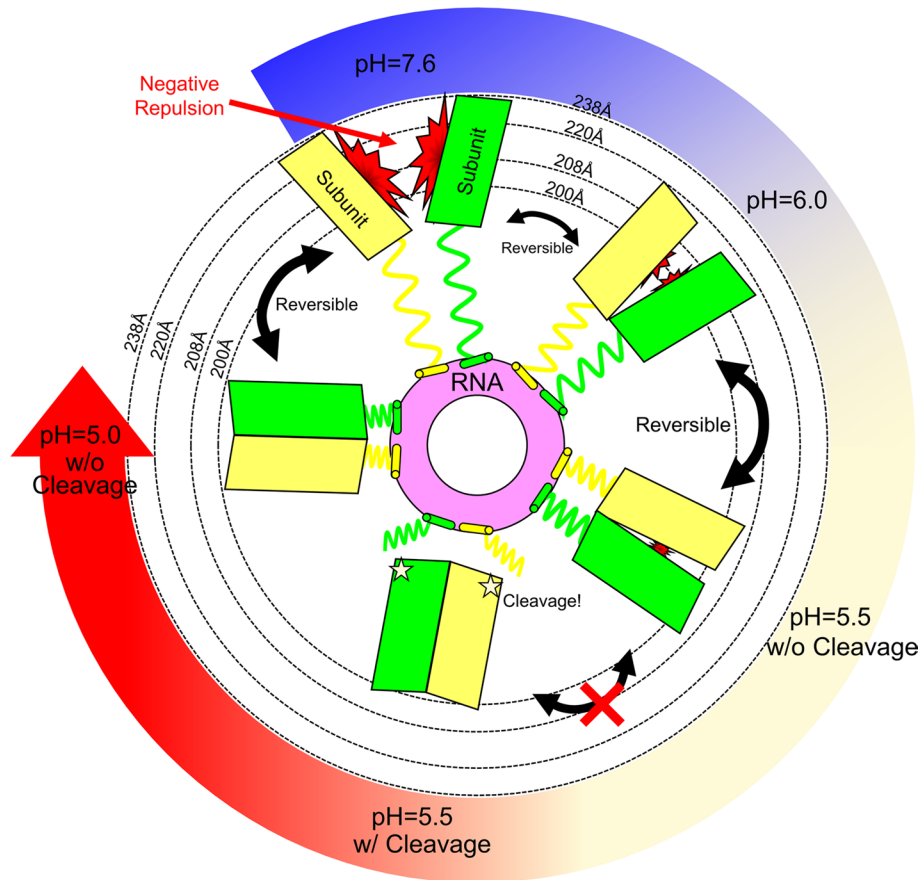


Fig. 11 A cartoon representation of the factors affecting NCV maturation and particle size. At pH 7.6, the dominant acidic residues on the surface of the subunits are negatively charged and the subunits repel each other. Interactions of the positively charged N- and C-terminal polypeptides (Fig. 1b) are portrayed as extended wavy lines in the cartoon and a hypothetical helix interacting with the RNA. These interactions maintain the particle integrity in spite of the repulsions. As the pH is lowered, hydrogen ions protonate the acidic residues,

lowering the charge and allowing the subunits to approach more closely with an associated reduction in radius. The process continues as the pH is lowered, initiating subunit cleavage at ~pH 5.8. As shown in Figure 10, at pH 5.5, the cleavages must occur to allow the particle to achieve the final mature radius. The entire process is reversible if a non-cleaving mutant (Asn570Thr) is used or if less than 10% of the subunits are cleaved at pH values above 5.5.

electrostatic interactions between the positively charged N-terminal 44 residues (Fig. 1b) and the packaged RNA, bringing a “balloons on a string” image to mind, with the balloons repulsed from each other by the negative charge. As the charge is reduced by adding protons to lower the pH, the subunits draw closer together with a decrease in radius. Below pH 5.8, the subunit reorganization has placed the catalytic residues of the cleavage site in some of the subunits into proximity for the chemical reactions to occur (Fig. 9).

Time-resolved cryo-EM analysis of particle maturation

A more detailed three-dimensional analysis of maturation was performed with a time-resolved cryo-EM study of particles in which the pH was changed from 7.6 to 5.0 in less than a second. The pH 5.0 particles were then flash-frozen at 3 minutes (15% of subunits cleaved), 30 minutes (50% of subunits cleaved), and 4 hours (80% of subunits cleaved) after lowering the pH. Complete cryo-EM data

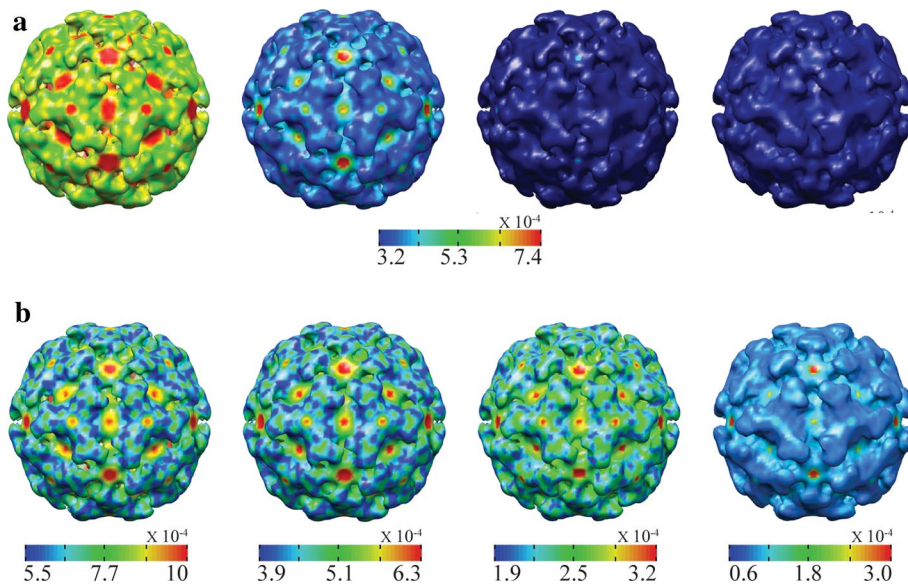


Fig. 12 Time-resolved maturation data sets [22] were used to extract dynamic information from NmV cryo-EM reconstructions using the variance method [35]. The reconstructed density of the capsids at each maturation state was solved *de novo* using the maximum-likelihood algorithm, which explicitly takes into account the continuous heterogeneity of the ensemble of particles present in the data set. The result describes the heterogeneity of the particle as a variance plotted at every voxel of the reconstructed density. This methodological approach allowed the analysis of the whole-particle dynamics during maturation, as shown by the surface coloring of the capsids. The

top row shows the variance for particles at 3 minutes, 40 minutes, 4 hours, and 3 days after lowering the pH from 7.6 to 5. They are all on the same scale. The bottom row shows the variance of each particle with its own scale showing variance differences within each particle. It is clear that at 3 minutes there is a large variation in the ensemble of particles; the variance is reduced after 40 minutes when approximately 50% of the subunits have been cleaved. There is little difference in the variance between 4 hours (80% of the subunits cleaved) and the fully mature state (95% of subunits cleaved).

sets at each time point were collected, resulting in subnanometer 3D reconstructions [22].

The first investigation of the data employed a method that determined the standard deviation of the particle population (color coded between 1.5 and 5.5 standard deviations over the population of particles on the grid) as a function of time and the number of cleavages (Fig. 12 top, all particles color coded on the same scale; bottom, each particle is color-coded on its own scale). At 3 minutes, the average particle had a standard deviation of 3.5 (green); at 30 minutes, 2.5 (light blue turquoise); and at 4 h, approximately 1.5 (deep blue). This demonstrates that the particles occupy a variety of conformations at the same size prior to the subunits being cleaved. As cleavages occur, the particles are less dynamic and reach a stable, uniform structure, which we call the “ground state”, at pH 5 [23]. The same behavior is demonstrated with static cryo-EM data in Figure 13, where the standard deviation is shown for the procapsid particle at pH 7.6, the Asn-Thr non-cleaving mutant at pH 5.0, and the fully mature particle at pH 5.0. The large standard deviation for the non-cleaving mutant at pH 5.0 is consistent with the fact that cleavage is required for the particle to reach the “ground state”; without cleavage it is sampling many structures that are higher on the energy landscape. Figure 10 shows the

same behavior at pH 5.5, where the particle size decreased as a function of the number of cleavages.

The time-resolved data described above were analyzed in greater detail by examining the volumes corresponding to the cleavage sites in the four subunits of the icosahedral asymmetric unit (determined from the X-ray structure model). A fourth data set was collected under identical conditions at 96 hours after lowering the particles to pH 5.0. These particles were fully cleaved and correspond to mature particles. The data for each of the time points were then individually scaled with the fully mature (96 hour) particle data to have an average density of zero. Difference density (fully mature density minus time-point density) was then computed at each cleavage site volume. While the overall average density was zero, local density volumes can be non-zero. As shown in Figure 14, the experiment showed the rate at which the active sites in the different subunits formed based on the difference density. At 3 minutes, density for the A and D sites was weak, indicating that those sites were already closely similar to the mature particle and were ready to cleave the polypeptide. B and C sites had large difference density, indicating that those sites had not yet formed completely. At 40 minutes, the B site density was considerably lower than it was at 3 minutes, indicating that the active site was well formed and ready to cleave. The C site difference

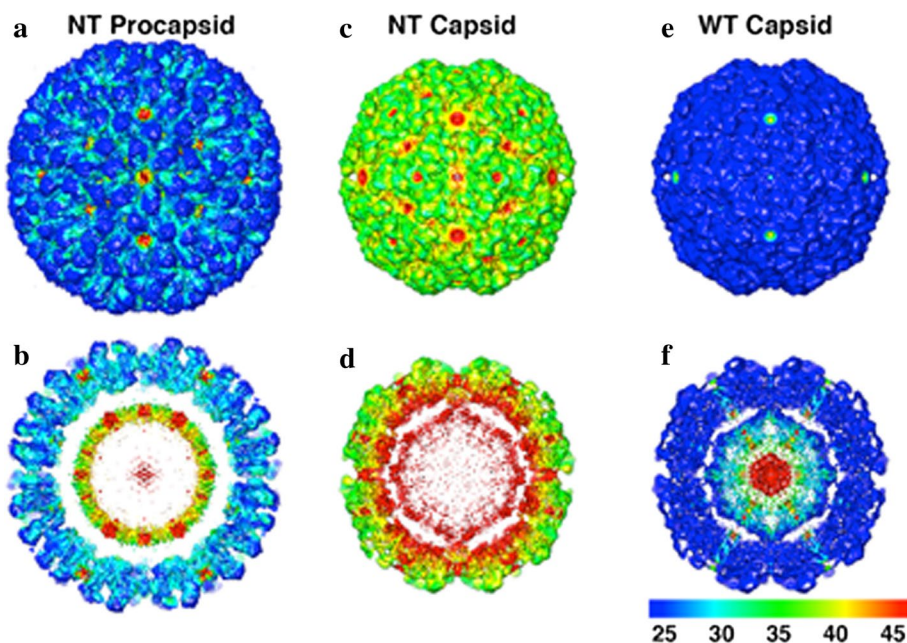


Fig. 13 Variance maps for the Asn570Thr mutant procapsid (left) at pH 7.6 and Asn570Thr (center) and capsid (right) at pH 5. The top row shows the outer surface, and the bottom row shows the cross section. Although the Asn570Thr procapsid has large holes and appears fragile, the ensemble of particles in the cryoEM experiment used in the reconstruction was largely uniform. The non-cleaving mutation in the procapsid has no effect on the structure, since cleavage does

not occur at pH 7.6. The Asn570Thr particles at pH 5 have a high variance caused by the lack of autocatalytic cleavage in this mutant. The ensemble of particles displays a large variation from the averaged density shown due to the inability of the particle to achieve the most stable state that requires cleavage. The fully cleaved mature capsid shows very low variance in the ensemble of particles used for the reconstruction, showing that they all have closely similar structures.

density was still quite significant, indicating that active site formation was still in process. The four-hour time point showed the A, B and D sites had minimal density, while C was still in the process of forming. Given that all four sites are formed from polypeptides that are closely similar in the final mature structure, the differences in the time-resolved experiment must result from differences in subunit annealing times that are dependent on their quaternary position [22]. The results explain the observed kinetics of cleavage, as displayed in cartoon form in Fig. 15.

Role of NoV particle maturation in infection

The structure and function of NoV maturation has been described as a biophysical phenomenon to this point. Here, we discuss the evidence for the role of maturation in virus infection. It is common for non-enveloped animal viruses to harbor a lytic peptide that is released into a target cell membrane (plasma or endosomal) to facilitate entry of either the particle or the genome into the cytoplasm of the cell [24]. The covalently released, but particle-associated gamma peptide that is the result of NoV maturation is a candidate for such a role.

Artificial, dye-filled membrane liposomes were employed to test this hypothesis (Fig. 16). Liposomes made from 1,2-dioleoyl-sn-glycero-3-phosphocholine (DOPC) and filled with the dye sulforhodamine B were employed for these experiments. Within the liposome, the dye self-quenches, and there is minimal fluorescence. When these liposomes are ruptured, they release dye and the unquenched fluorescence is a readout of the effect of reagents on the liposome membrane. Figure 16b illustrates, in cartoon fashion, the expected outcome if virus particles are able to lyse the liposome membrane. Experiments were performed with mature NoV particles that were placed in the liposome solution at different pH values. A dramatic dependence on pH for liposome lytic activity was observed with maximum activity at pH 8 and above [25]. These results were unexpected, as similar experiments performed previously with FHV, also harboring a covalently independent, particle-associated gamma peptide following maturation, showed maximum lytic activity at pH 5, consistent with studies of FHV demonstrating that the particles or genome enter the cytoplasm through endosomal membranes [26]. Following the determination of the pH of maximum lytic activity for NoV mature particles, comparisons were made between procapsid particles and mature particles at pH 8. Procapsids demonstrated no lytic activity, while mature particles

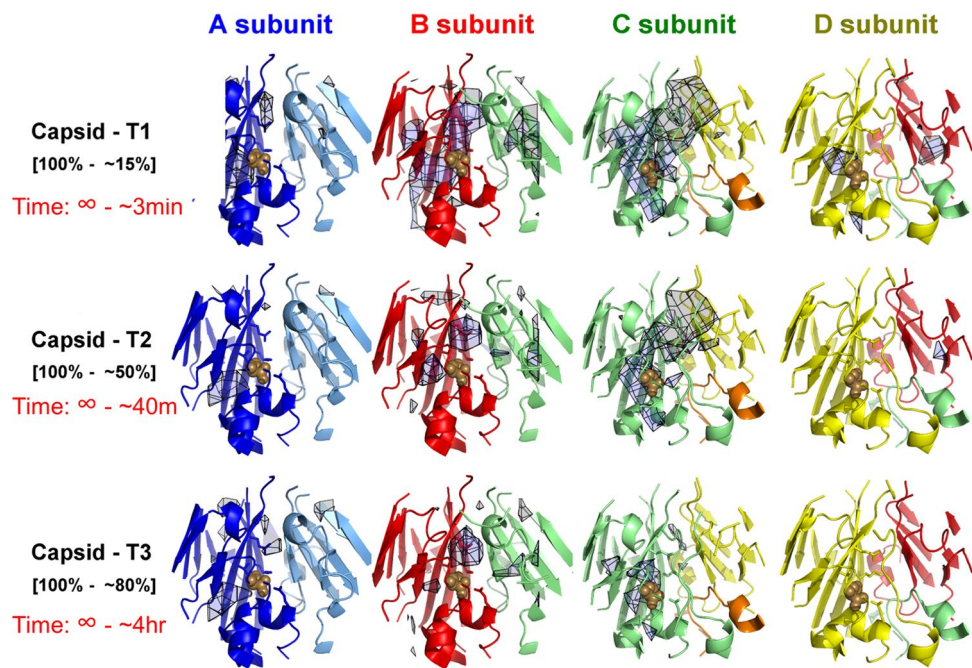
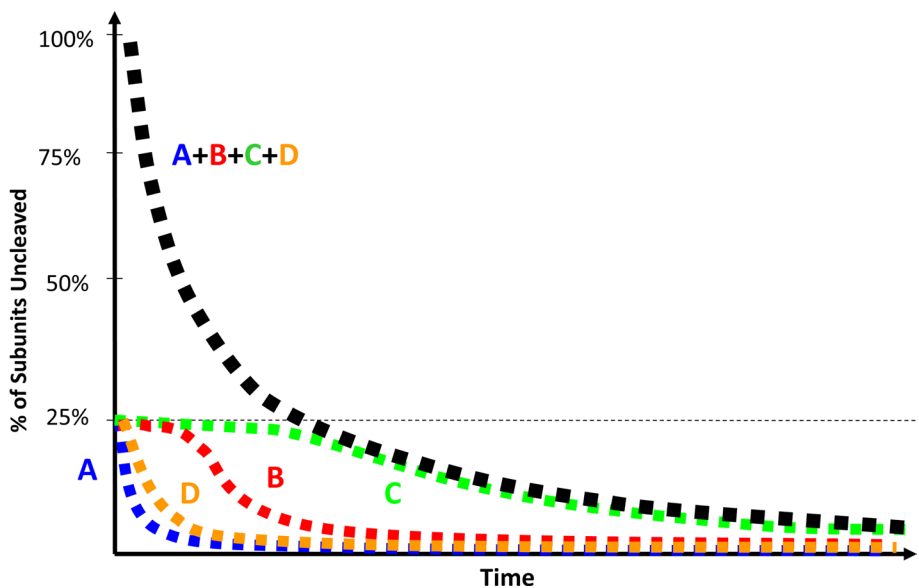


Fig. 14 Conventional difference electron scattering density maps computed by comparing cryoEM reconstructions of fully cleaved mature capsid and particles flash-frozen at 3 minutes, 40 minutes, and 4 hours after lowering the pH from 7.6 to 5.0. The fraction of subunits is shown just below the time point. The regions shown for each subunit at each time point correspond to the cleavage site volume as determined from the model based on the high-resolution X-ray structure of the capsid. Low difference density implies close similarity between fully cleaved capsid and the subunits at different time points, while large difference density indicates that the subunits at those time points are different from those in the mature capsid. Examination

of the density at 3 minutes shows that the structures of the A and D subunits are closely similar to those in the capsid (low difference density), indicating that the cleavage site has formed, while the B subunit has larger density and the C subunit has the largest difference density, indicating substantial differences between the B and C subunits and capsid. At 40 minutes, the A, B and D subunit densities are weak, while the large C subunit density persists. At 4 hours, the density is weak for all four subunits, indicating well-formed active sites as expected, with 80% of the subunits cleaved. These data explain the kinetics of cleavage observed in Figure 7.

Fig. 15 A cartoon representation of the cleavage kinetics observed in Figure 7 with the overall curve described in terms of events for each subunit based on the data in Figure 14



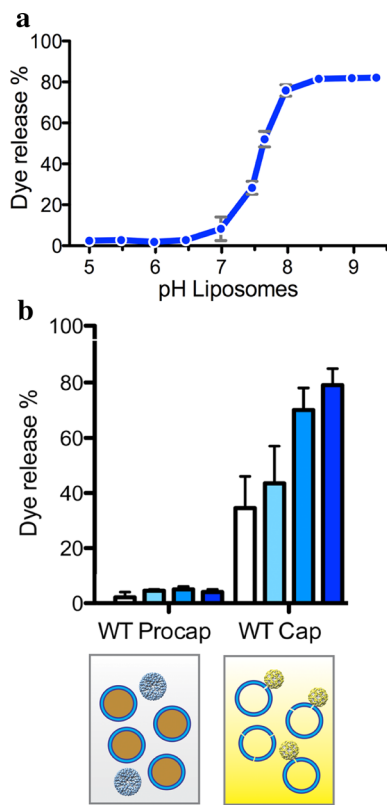


Fig. 16 Artificial membrane liposomes as an indicator of lytic activity in virus particles. Top: The pH profile of lytic activity for mature N_oV VLP capsids employing liposomes made from 1,2-dioleoyl-sn-glycero-3-phosphocholine (DOPC) filled with sulforhodamine B. 100% lytic activity was defined based on treatment with Triton X-100, which is assumed to release all of the dye from the liposomes. Middle (right): Comparison of lytic activity of procapsids and mature capsids. Procapsids (uncleaved subunits) do not release dye, while mature particles (cleaved subunits) do, demonstrating that the gamma peptide must be covalently independent for lytic activity to occur. Different ratios of particles to liposomes were employed, showing that dye release is proportional to the number of particles in solution. Bottom: A cartoon representation of liposomes made from a defined phospholipid by sonicating the lipid and allowing reassembly into roughly spherical particles. When done in the presence of a dye (sulforhodamine B in this case), the dye is packaged in the liposome. When dye-loaded liposomes are separated from the non-packaged dye, there is little fluorescence due to self-quenching of the dye within the liposome. When there is lytic activity, the liposome is ruptured and dye escapes, generating a strong fluorescence signal.

displayed activity proportional to the number of particles input [25]. A similar effect was later observed for the closely related, authentic *Helicoverpa armigera* stunt virus (HasV), which required an alkaline environment for the binding and entry into cells [27]. Three conclusions were drawn from the experiments. First, given the high pH of activity, it is likely that the particles enter through the plasma membrane and not through endosomes. Second, the gamma peptides must be transiently exposed at pH 8, as the structure shows that they are internal and not accessible to the surface of the

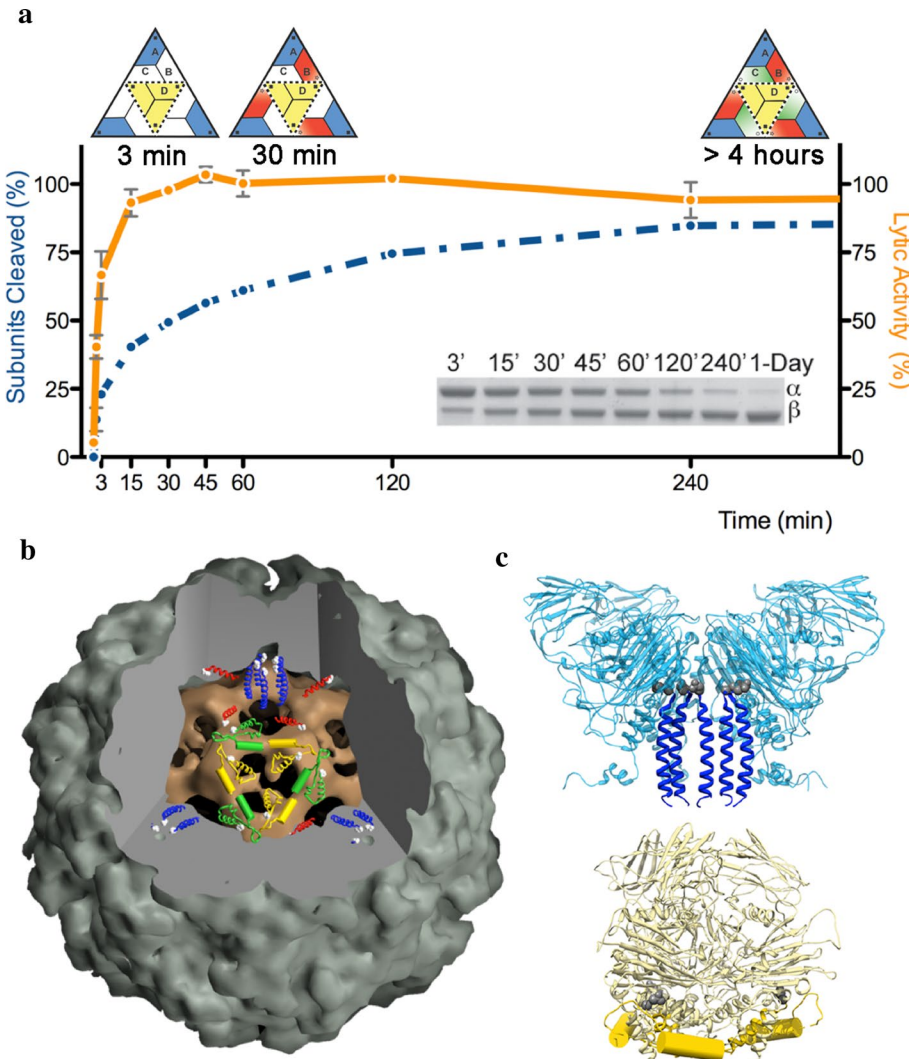
particle. Third, the gamma peptides must be covalently independent to have activity. The last conclusion was confirmed with the Asn570Thr mutant, which does not cleave at low pH. After lowering the pH to 5.0 to put the particle in the compact form, the particles were suddenly exposed to pH 8.0 in the presence of liposomes before they could expand. There was no dye release. These data support the hypothesis that covalently free gamma peptides are required for membrane interactions and associated delivery of the particles or genome to the cytoplasm [25].

A final question addressed in the liposome studies was the subunit source of the lytic gamma peptide, A, B, C, or D. Time-resolved analysis of cleavage demonstrated that A and D must cleave before B and C, based on the rate of cleavage site formation. A time-resolved study of dye release would indicate when lytic activity occurred relative to the rates of cleavage. Figure 17a shows that virtually full lytic activity is achieved in 15 minutes after lowering the pH to 5.0 and raising it to pH 8.0 after 2 minutes. Figure 17b shows the disposition of gamma peptides in the particle. A subunits form pentamers, and the gamma peptides of these subunits are closely associated near the 5-fold axes and can be transiently exposed through the 5-fold axes to interact with membranes. D subunits are an integral part of the capsid and form part of the molecular switch that stabilizes interactions between the C and D subunits. It is impossible for this gamma peptide to be released, but cleavage early for D subunits allows them to fully lodge into the interface and stabilize the particle. Thus, A subunits provide the lytic peptides for membrane rupture [25].

A model for the N_oV life cycle

Fully mature N_oV virions are first ingested into lepidopteran larvae that have a progressively more alkaline environment moving from the entrance of the digestive tract to the midgut, where the pH is in excess of 11 [28]. It is in this environment where N_oV gamma peptide lytic activity is the greatest and where the virus is likely to enter the midgut cells through the plasma membrane, releasing the RNA1 and RNA2 components of the genome. Like all RNA viruses investigated, RNA1 is translated first to generate the RNA-directed polymerase (RDP), which then replicates the RNA molecules to produce large pools for translation. Capsid protein is produced in large quantities and proceeds to assemble into provirions packaging RNA1 and RNA2, as described above, in SF21 insect cells employed for expression. Maturation must then occur to generate infectious virions. This has been challenging to observe due to the lack of a cell line to study the entire virus life cycle. Some insight was gained when a tetravirus was expressed in *Saccharomyces cerevisiae* cells. Virus-like particles were shown to assemble as procapsids that matured spontaneously

Fig. 17 Top: Time-resolved analysis of dye released (gold solid line) compared to the fraction of subunits cleaved (dashed blue line). The top portion of the panel depicts the cleavage of each subunit type based on the data from Figure 14. Full lytic activity is achieved in ~15 minutes when only A and D subunits have fully formed the cleavage site. The bottom panel of the figure shows the location of the visible portions of the gamma peptide in the A and D subunits, both with respect to the whole particle (left) and, at higher magnification, the adjacent subunits (right). The D subunit gamma peptide is an integral part of the capsid and functions as a switch to maintain the C and D subunit contact as a flat surface. Its cleavage is likely to stabilize the particle. Only the A subunit gamma peptide can contribute to the lytic activity and it provides 100% of this activity after only 15 minutes of initiating maturation by lowering the pH from 7.6 to 5.0.



in vivo as the cells began to age. Growth of *Saccharomyces cerevisiae* cells in the presence of hydrogen peroxide or acetic acid, which induced apoptosis in the yeast cells, resulted in virus-like particle maturation. The results demonstrate that assembly-dependent maturation of tetravirus procapsids *in vivo* is linked to the onset of apoptosis in yeast cells [29]. The reduction in pH required for tetraviral maturation may be the result of cytosolic acidification, which is associated with the early onset of programmed cell death in infected cells. Mature, infectious N_oV particles are probably released when the cells are ruptured by the large number of virus particles in the cell, as there are no known virus-encoded mechanisms to release the particles.

Applications of N_oV conformational changes

N_oV has potential to be a model for the development of versatile and precise dynamic protein assemblies that can adapt to different environments and applications. Obtaining more details of the maturation process of this virus will be critical for this purpose. N_oV capsid VLPs have been shown to resist the harsh conditions of simulated gastrointestinal fluids, with digestive enzymes and acidic conditions (pH 1.2 - 4.0), while procapsids were less stable [30]. These differences are linked to the conformational

changes during the maturation of the virus. Properties such as the porosity of procapsids, which may facilitate cargo loading, and the robustness of capsids, makes NoV VLPs a promising candidate for protein cages for drug delivery systems. Additionally, some of its components, like the gamma peptide, have already been used for the delivery of quantum dots into cells directly through the plasma membrane, which has great potential for further biotechnology applications [31, 32].

Conclusions

The NoV maturation scheme provides a novel opportunity to investigate, at near-atomic resolution, the process by which a particle transitions from a non-infectious provirion to the infectious virion. In principle, this can be done by populating an arbitrary number of intermediate states by adjusting the pH and determining high-resolution cryo-EM structures of each step in the maturation. Since the progression involves large-scale changes in protein quaternary structure as well as significant changes in tertiary structure, it provides an opportunity to understand the driving forces involved in these modifications at a very fine level. The prospect for unforeseen details is high because both the quaternary and tertiary structure changes are occurring in four versions of the same polypeptide with differences attributed primarily to four distinct, but quasi-equivalent, quaternary structure environments. The studies described above demonstrated the dramatically different roles the same amino acid sequences have in the different mature subunits and showed that they are essentially equivalent in the procapsid. How and when do they differentiate, with A subunits forming a pentameric bundle of helices and C and D helices forming a molecular switch to stabilize the capsid? Why do A and D cleavage sites form more rapidly than B and C after lowering the pH? What are the details of the scaffold formed by uncleaved subunits, which slowly changes, allowing the particle to change size? There is still more to learn from this remarkable system.

References

- Qin J, Gronenborn AM (2014) Weak protein complexes: challenging to study but essential for life. *FEBS J* 281(8):1948–1949. <https://doi.org/10.1111/febs.12744>
- Wang JC, Chen C, Rayaprolu V, Mukhopadhyay S, Zlotnick A (2015) Self-assembly of an alphavirus core-like particle is distinguished by strong intersubunit association energy and structural defects. *ACS Nano* 9(9):8898–8906. <https://doi.org/10.1021/acsnano.5b02632>
- Hendrix RW, Johnson JE (2012) Bacteriophage HK97 capsid assembly and maturation. *Adv Exp Med Biol* 726:351–363. https://doi.org/10.1007/978-1-4614-0980-9_15
- Pornillos O, Ganser-Pornillos BK (2019) Maturation of retroviruses. *Curr Opin Virol* 36:47–55. <https://doi.org/10.1016/j.covir.2019.05.004>
- Sirohi D, Kuhn RJ (2017) Zika virus structure, maturation, and receptors. *J Infect Dis* 216(suppl_10):S935–S944. <https://doi.org/10.1093/infdis/jix515>
- Ghosh AK, Osswald HL, Prato G (2016) Recent progress in the development of HIV-1 protease inhibitors for the treatment of HIV/AIDS. *J Med Chem* 59(11):5172–5208. <https://doi.org/10.1021/acs.jmedchem.5b01697>
- Plevka P, Battisti AJ, Junjhon J, Winkler DC, Holdaway HA, Keelapang P, Sittisombut N, Kuhn RJ, Steven AC, Rossmann MG (2011) Maturation of flaviviruses starts from one or more icosahedrally independent nucleation centres. *EMBO Rep* 12(6):602–606. <https://doi.org/10.1038/embor.2011.75>
- Olson N, Baker T, Johnson J, Hendry D (1990) The three-dimensional structure of frozen-hydrated *Nudaurelia capensis* beta virus, a $T = 4$ insect virus. *J Struct Biol* 105(1–3):111–122
- Cavarelli J, Bomu W, Liljas L, Kim S, Minor W, Munshi S, Muchmore S, Schmidt T, Johnson J (1991) Crystallization and preliminary structure analysis of an insect virus with $T=4$ quasi-symmetry: *Nudaurelia Capensis w* virus. *Acta Crystallogr B* 47:23–29
- Agrawal DK, Johnson JE (1992) Sequence and analysis of the capsid protein of *Nudaurelia capensis omega* virus, an insect virus with $T = 4$ icosahedral symmetry. *Virology* 190(2):806–814
- Munshi S, Liljas L, Cavarelli J, Bomu W, McKinney B, Reddy V, Johnson JE (1996) The 2.8 Å structure of a $T = 4$ animal virus and its implications for membrane translocation of RNA. *J Mol Biol* 261(1):1–10. <https://doi.org/10.1006/jmbi.1996.0437>
- Helgstrand C, Munshi S, Johnson JE, Liljas L (2004) The refined structure of *Nudaurelia capensis omega* virus reveals control elements for a $T = 4$ capsid maturation. *Virology* 318(1):192–203. <https://doi.org/10.1016/j.virol.2003.08.045>
- Agrawal DK, Johnson JE (1995) Assembly of the $T = 4$ *Nudaurelia capensis omega* virus capsid protein, post-translational cleavage, and specific encapsidation of its mRNA in a baculovirus expression system. *Virology* 207(1):89–97. <https://doi.org/10.1006/viro.1995.1054>
- Schneemann A, Dasgupta R, Johnson JE, Rueckert RR (1993) Use of recombinant baculoviruses in synthesis of morphologically distinct viruslike particles of flock house virus, a nodavirus. *J Virol* 67(5):2756–2763
- Canady MA, Tihova M, Hanzlik TN, Johnson JE, Yeager M (2000) Large conformational changes in the maturation of a simple RNA virus, *nudaurelia capensis omega* virus (NomegaV). *J Mol Biol* 299(3):573–584. <https://doi.org/10.1006/jmbi.2000.3723>
- Canady MA, Tsuruta H, Johnson JE (2001) Analysis of rapid, large-scale protein quaternary structural changes: time-resolved X-ray solution scattering of *Nudaurelia capensis omega* virus (NomegaV) maturation. *J Mol Biol* 311(4):803–814. <https://doi.org/10.1006/jmbi.2001.4896>
- Lee KK, Tsuruta H, Hendrix RW, Duda RL, Johnson JE (2005) Cooperative reorganization of a 420 subunit virus capsid. *J Mol Biol* 352(3):723–735. <https://doi.org/10.1016/j.jmb.2005.07.024>
- Konarev PV, Volkov VV, Sokolova AV, Koch MHJ, Svergun DI (2003) Primus: a Windows PC-based system for small-angle scattering data analysis. *J Appl Cryst* 36:1277–1282. <https://doi.org/10.1107/S0021889803012779>
- Matsui T, Lander G, Johnson JE (2009) Characterization of large conformational changes and autoproteolysis in the maturation of a $T=4$ virus capsid. *J Virol* 83(2):1126–1134. <https://doi.org/10.1128/JVI.01859-08>
- Taylor DJ, Krishna NK, Canady MA, Schneemann A, Johnson JE (2002) Large-scale, pH-dependent, quaternary structure changes in an RNA virus capsid are reversible in the absence of

- subunit autoproteolysis. *J Virol* 76(19):9972–9980. <https://doi.org/10.1128/jvi.76.19.9972-9980.2002>
21. Matsui T, Tsuruta H, Johnson JE (2010) Balanced electrostatic and structural forces guide the large conformational change associated with maturation of $T = 4$ virus. *Biophys J* 98(7):1337–1343. <https://doi.org/10.1016/j.bpj.2009.12.4283>
 22. Matsui T, Lander GC, Khayat R, Johnson JE (2010) Subunits fold at position-dependent rates during maturation of a eukaryotic RNA virus. *Proc Natl Acad Sci USA* 107(32):14111–14115. <https://doi.org/10.1073/pnas.1004221107>
 23. Wang Q, Matsui T, Domitrovic T, Zheng Y, Doerschuk PC, Johnson JE (2013) Dynamics in cryo EM reconstructions visualized with maximum-likelihood derived variance maps. *J Struct Biol* 181(3):195–206. <https://doi.org/10.1016/j.jsb.2012.11.005>
 24. Banerjee M, Johnson JE (2008) Activation, exposure and penetration of virally encoded, membrane-active polypeptides during non-enveloped virus entry. *Curr Protein Pept Sci* 9(1):16–27
 25. Domitrovic T, Matsui T, Johnson JE (2012) Dissecting quasi-equivalence in nonenveloped viruses: membrane disruption is promoted by lytic peptides released from subunit pentamers, not hexamers. *J Virol* 86(18):9976–9982. <https://doi.org/10.1128/JVI.01089-12>
 26. Odegard AL, Kwan MH, Walukiewicz HE, Banerjee M, Schneemann A, Johnson JE (2009) Low endocytic pH and capsid protein autocleavage are critical components of Flock House virus cell entry. *J Virol* 83(17):8628–8637. <https://doi.org/10.1128/JVI.00873-09>
 27. Penkler DL, Jiwaji M, Domitrovic T, Short JR, Johnson JE, Dorrington RA (2016) Binding and entry of a non-enveloped $T=4$ insect RNA virus is triggered by alkaline pH. *Virology* 498:277–287. <https://doi.org/10.1016/j.virol.2016.08.028>
 28. Dow JA (1992) pH gradients in lepidopteran midgut. *J Exp Biol* 172(Pt 1):355–375
 29. Tomasicchio M, Venter PA, Gordon KH, Hanzlik TN, Dorrington RA (2007) Induction of apoptosis in *Saccharomyces cerevisiae* results in the spontaneous maturation of tetravirus procapsids in vivo. *J Gen Virol* 88(Pt 5):1576–1582. <https://doi.org/10.1099/vir.0.82250-0>
 30. Berardi A, Castells-Graells R, Lomonosoff GP (2020) High stability of plant-expressed virus-like particles of an insect virus in artificial gastric and intestinal fluids. *Eur J Pharm Biopharm* 155:103–111
 31. Merkl JP, Safi M, Schmidtke C, Aldeek F, Ostermann J, Domitrovic T, Gartner S, Johnson JE, Weller H, Mattoussi H (2019) Small protein sequences can induce cellular uptake of complex nanohybrids. *Beilstein J Nanotechnol* 10:2477–2482. <https://doi.org/10.3762/bjnano.10.238>
 32. Safi M, Domitrovic T, Kapur A, Zhan N, Aldeek F, Johnson JE, Mattoussi H (2017) Intracellular delivery of luminescent quantum dots mediated by a virus-derived lytic peptide. *Bioconjug Chem* 28(1):64–74. <https://doi.org/10.1021/acs.bioconjchem.6b00609>
 33. Taylor DJ, Johnson JE (2005) Folding and particle assembly are disrupted by single-point mutations near the autocatalytic cleavage site of *Nudaurelia capensis* omega virus capsid protein. *Protein Sci* 14(2):401–408. <https://doi.org/10.1110/ps.041054605>
 34. Stephenson RC, Clarke S (1989) Succinimide formation from aspartyl and asparaginyl peptides as a model for the spontaneous degradation of proteins. *J Biol Chem* 264(11):6164–6170
 35. Doerschuk PC, Gong Y, Xu N, Domitrovic T, Johnson JE (2016) Virus particle dynamics derived from CryoEM studies. *Curr Opin Virol* 18:57–63. <https://doi.org/10.1016/j.coviro.2016.02.011>

Publisher's Note Springer Nature remains neutral with regard to jurisdictional claims in published maps and institutional affiliations.